Critical-state-model parameters of polycrystalline $YBa_2Cu_3O_7$: Critical current in thin slabs and field penetration in hollow cylinders

P. Fournier* and M. Aubin
Département de Physique and Centre de Recherche en Physique du Solide, Université de Sherbrooke, Sherbrooke, Québec, CANADA, J1K 2R1

M.A.R. LeBlanc
Département de Physique, Université d'Ottawa, Ottawa, Ontario, CANADA, K1N 6N5
(Received 12 May 1994)

We compare the parameters of the generalized critical-state model (GCSM) used to reproduce data obtained from two independent measurements: the critical current of thin slabs and the field penetration in a hollow cylinder, both as a function of the applied magnetic field and temperature. We obtain a good correspondence between the parameters for a thin slab and those for a hollow cylinder in the case of fully oxygenated material. From critical-current measurements, we also observe that the temperature dependence of the GCSM parameters is affected by the quality of the junctions (their resistance) and the level of oxygenation at the surface of the grains. The influence of the intergrain lower critical field in the determination of I_c is also considered.

INTRODUCTION

The initial studies of the transport and magnetic properties of polycrystalline high-critical-temperature (high-T_c) superconductors have revealed their weak-link nature.[1–4] As an example, the critical current (I_c) decreases abruptly with the applied magnetic field,[1,5,6] being affected by a field as low as 5 G. This feature can be analyzed using the fact that each grain boundary behaves as a Josephson junction.[7] In the presence of a small magnetic field, Josephson vortices first penetrate the intergrain regions at the surface of the sample. Because there is a disordered array of Josephson junctions, these vortices can be pinned:[7–10] this gives rise to a field profile in the sample and corresponding induced macroscopic currents, which are observed through the low-field hysteresis in the magnetization[2] (for more details, see Ref. 11). As one increases the applied magnetic field, the local field in the intergrain region becomes more and more uniform and the grains are virtually decoupled (the width of the low-field hysteresis cycle, ΔM, tends to zero). Once the lower critical field of the grains, H_{c1g}, is exceeded, Abrikosov vortices begin to penetrate the grains: another hysteresis cycle appears and is related to the intragrain pinning.

In the work presented here, we concentrate on the study of the *intergrain* pinning, which determines the field dependence of the macroscopic (sample) critical current density, $J_{cj}(H)$. We present the results of two independent experiments: the measurement of the critical current (I_c) in thin slabs and the field penetration in a hollow cylinder[12–14] (measured as $H_{\rm cent}$), both as a function of the applied magnetic field and temperature. We reproduce the $I_c(H_a)$ data using a method first presented by Müller, Matthews, and Driver[15] for polycrystalline $YBa_2Cu_3O_7$, which can be followed in more detail in Ref. 16 (in this work, LeBlanc also includes the contributions of the reversible currents when H_{c1} cannot be neglected). This procedure uses the critical state model to determine $I_c(H_a)$.[17] Typical results are well illustrated for several critical state models in Ref. 15 and can explain the dependence of I_c with the sample dimensions as seen by several authors.[18] The best results are obtained with an H^{-2} dependence for $J_{cj}(H)$.

Here, we use the generalized critical state model (GCSM),[19] which gives the critical current density as a function of the local magnetic field $H(r)$:

$$J_{cj}(H) = \frac{J_{c0}}{[1+\mid H(r)\mid/H_0]^n}\ , \tag{1}$$

where n, J_{c0}, and H_0 are the three parameters that we obtain as a function of temperature by fitting $I_c(H_a)$. Then, we compare them with the ones determined with a hollow cylinder[14] of the same material. We finally extend our analysis to explain the effect of various heat treatments. This allows us to relate important characteristics of the microstructure to the GCSM parameters.

EXPERIMENTAL SETUP AND PROCEDURES

Sample preparation

The polycrystalline $YBa_2Cu_3O_7$ pellets are prepared by the usual sintering route, using Y_2O_3 , $BaCO_3$ and CuO as starting materials. The nominal 1:2:3 composition is first calcined at 900 °C for 48 h in air (with an intermediate grinding after 24 h) and furnace cooled to room temperature. The resulting powder is ground and pressed into pellets of 12.5-mm diameter and approximately 2-mm thickness. The batch of 10 to 15 pellets

 ©1994 The American Physical Society

are then treated at 940 °C for 48 h in ultra-pure oxygen (UP O_2) at 1 atm. While decreasing the temperature, a further step at 410 °C for 48 h in the same atmosphere is required to ensure saturation with respect to the oxygen content. Two pellets of the batch are kept for critical current measurements and for characterizations (x rays and resistivity). The rest is used to build the hollow cylinder. This ensures that both experiments are done with samples made of an identical grain size distribution. The powder x-ray diffraction (Cu $K\alpha$) reveals a single orthorhombic phase[20] for all samples.

Measuring $I_c(H_a)$

For this experiment, we cut the first two $YBa_2Cu_3O_7$ pellets in the shape of long thin slabs with typical dimensions of 0.2–0.4-mm thickness, 1.2–2-mm width, and 10-mm length. A thin slab is used here to avoid complications due to the geometry: in our case, as one increases the transport current along the length, the dominant contribution to the self-field appears along the width as shown in Refs. 15 and 16. Six contact pads are made by applying silver paste which is then briefly annealed at 900 °C. The sample is then oxygenated at 410 °C in UP O_2 for various periods.[21] The additional heat treatment at 900 °C implies a decrease of the oxygen content. To return to the saturated level of oxygen in the thin slabs, several heat treatments at 410 °C are tried. Here, we compare the results from three samples shown in Table I. Sample $6H$ is treated for six hours at 410 °C in UP O_2. After the I_c measurements, we use the same sample to obtain $D6H$: $6H$ is first left in the degrading ambient atmosphere for 1 month. Then, new Ag pads are applied and are heat treated at 900 °C. The oxygenation step at 410 °C is extended to 48 h to ensure sufficient oxygen content. Finally, $48H$ is a sample from the same root pellet but with a heat treatment at 410 °C lasting 48 h. Table I also shows the dimensions of the slabs, their resistivity at 100 K and their sligthly different T_{c0} (at which, $\rho = 0$) as determined by the resistivity measurement.

In Ref. 22, we present the experimental technique used for the measurement of the critical current at several temperatures, while the sample remains in direct contact with liquid nitrogen (LN_2). In summary, the sample is first immersed in LN_2 in zero (earth) field. The LN_2 container is sealed such that one can then increase the nitrogen gas pressure or pump on the liquid to achieve the desired temperature above or below 77 K, respectively. Once the temperature of the sample is stabilized, one can proceed with the measurement of the V-I curves for an increasing applied magnetic field. The critical current is determined using a voltage criterion of 1 μV (Ref. 23) (giving approximately 2 μV cm^{-1} for all the samples). The magnetic field is applied along the width such that the critical state (and the field profile) is established along the thickness: in the analysis, we focus on the applied field and the self-field along the width.

Measuring $H_{cent}(H_a)$

The hollow cylinders (HC's) are obtained by stacking up several pellets. A small hole is drilled initially in each pellet and then gradually enlarged by sandblasting giving a wide range of wall thicknesses for this fragile material (from 1 to 4 mm). The central field is detected as a function of the applied magnetic field using a Hall probe of 10^{16} cm^{-3} n-type GaAs. All the measurements are made with the sample initially cooled in zero (earth) field by a closed cycle refrigerator (10 to 300 K). The field is applied along the symmetry axis of the cylinder and never exceeds the lower critical field of the grains (H_{c1g}).[14] In Table I, we also add general information about the geometry, resistivity at 100 K and the T_c of HC.

RESULTS AND DISCUSSION

Critical current of thin slabs

Figure 1 presents an example of the critical current of our samples ($48H$) as a function of the applied magnetic field for three different temperatures. As already observed,[1,5,6,15] I_c presents an abrupt decrease for low applied fields. In the inset of Fig. 1, it is also shown that the temperature dependence of I_{c0}/S is sample-dependent (here, I_{c0} is the zero-field critical current and S is the cross section of the slab). One can also observe (not shown here) that the field at which $I_c = I_{c0}/2$ is different for each sample at a given temperature and increases generally with I_{c0}. Both observations prove that the extent of the 410 °C treatment has a direct impact on the quality of the samples and should have a very important effect on the values of the GCSM parameters.

TABLE I. Details of the sample preparations and general properties.

Sample	410 °C treatment duration (h)	Dimensions (mm^3)	ρ(100 K) ($\mu\Omega$ cm)	T_{c0} (K)
$6H$	6	0.36×1.20×12	300	90
$D6H$	48, on $6H$ after air degrad. for 1 month	0.36×1.20×12	500	89
$48H$	48	0.21×2.04×12	130	91
HC	no additional heat treatment	wall thickness = 4 mm ext. diameter = 12.5 mm length = 9 mm	150	91

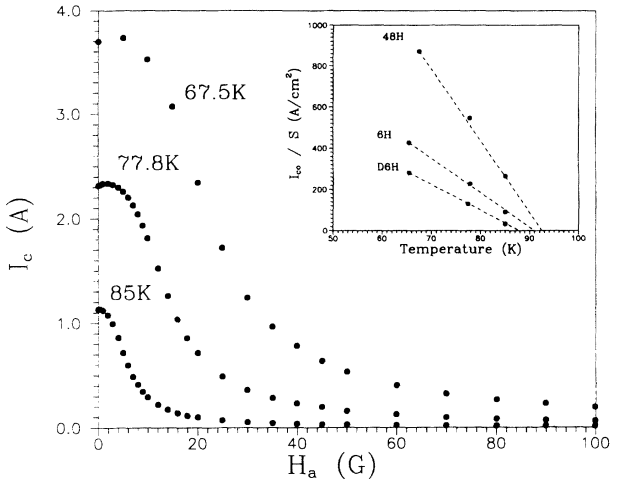

FIG. 1. Critical current as a function of the applied magnetic field for $48H$ at various temperatures. The inset shows the transport critical current density at zero field (I_{c0}/S) as a function of temperature for $6H$, $D6H$, and $48H$.

In Fig. 2, we reproduce the magnetic field dependence of some $I_c(H_a)$ curves at different temperatures using a modified version of the fitting technique already presented in detail by Müller, Matthews, and Driver.[15] To perform the fit, we introduce the measured I_{c0}, which is related to the full penetration field H_p of the slab[16] as can be easily deduced from the GCSM.[19] Neglecting the contribution of H_{c1j}, the lower critical field of the junctions, we then obtain

$$I_{c0} = 2YH_p, \tag{2}$$

where Y is the width of the slab. A study of Figs. 2(a) and 2(b) leads one to note that, as the quality of the sample improves and the temperature of the measurement decreases (I_{c0} increases), the fits diminish in quality, whatever the parameters. This problem will be discussed below.

Field penetration in a hollow cylinder

The procedure used to fit the hollow cylinder data is described elsewhere.[14] In summary, we determine H_{cent} as a function of the effective (or surface) field H_{eff}. Because the length of the cylinder is comparable to its diameter, a significant change in the applied field is expected from the magnetic field produced by the induced currents: we take this into account by introducing a demagnetizing factor. Then, one has to evaluate the magnetization of the cylinder as a function of H_{eff} , multiplies it by the demagnetizing factor N and add vectorially the demagnetizing field to the applied one. One can then obtain the entire hysteresis loop, H_{cent} as a function of H_a. Several features of the demagnetizing effects with this type of geometry can be reproduced, and we refer the reader to the Ref. 14 for more details.

The GCSM parameters

At this point, we can compare the parameters extracted from the critical current in thin slabs and those obtained from the hollow cylinder.[14] We underline first that the exponent n is the same ($n = 2.0 \pm 0.2$) in both cases and does not depend on temperature (from 20 K to T_c). Moreover, this parameter is independent of the extent of the 410 °C treatment and even the degradation in air. This suggests that it is related to the geometrical aspects of the microstructure and that it is independent of the typical superconducting parameters for a Josephson junction, such as the coupling energy between two adjacent superconducting grains.[7] This value of $n = 2.0$ reflects the fact that the interfaces of the junctions present a wide distribution of angles with respect to the local field $\mathbf{H}(\mathbf{r})$ in the sample giving a field dependence of H^{-2} (see Refs. 15, 24, and 25).

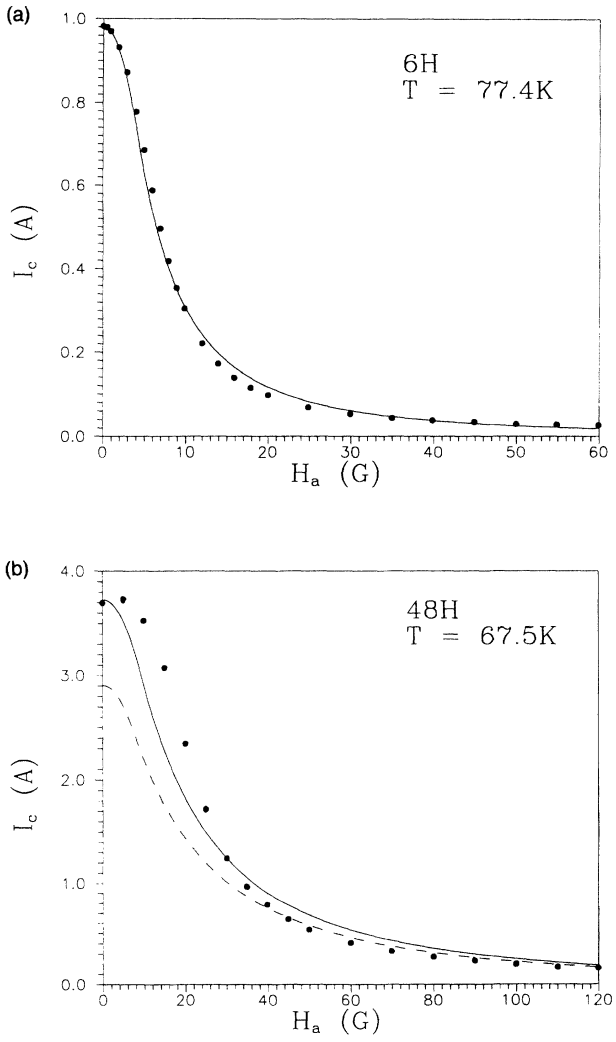

FIG. 2. Fits of $I_c(H_a)$ for (a) $6H$ at 77.4 K and (b) $48H$ at 67.5 K. Also shown in (b), the dashed I_c curve obtained with the interpolated hollow cylinder (HC) parameters. Here, $n = 2$, and J_{c0} and H_0 are shown in Figs. 3 and 4, respectively.

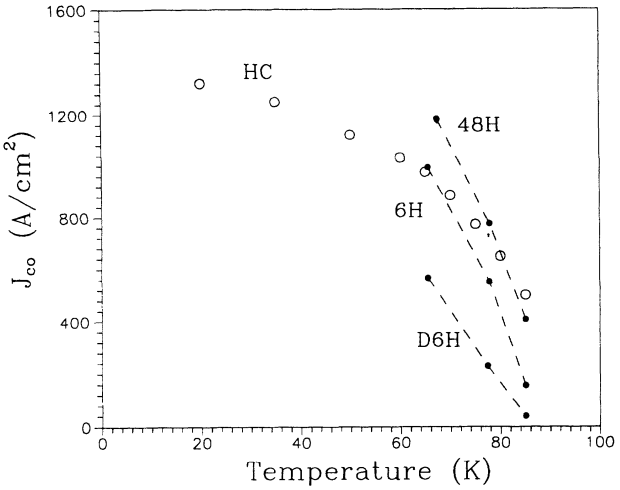

FIG. 3. J_{c0} as a function of temperature for $D6H$, $6H$, $48H$, and HC. The dashed lines are guides to the eye.

Figures 3 and 4 present the temperature dependence of J_{c0} and H_0, respectively, for the three thin slabs and the hollow cylinder. We first observe that the parameters for the $48H$ slab correspond mostly to the ones obtained from the hollow cylinder (HC). This excludes the point at 67.5 K, which is influenced by the neglected contribution of the reversible currents (see below). With the exception of the latter contribution, this means that the GCSM model, or any other critical-state model capable of fitting one of the experiments, describes fully the magnetic and transport properties of polycrystalline $YBa_2Cu_3O_7$ in low fields.

The degradation in air ($D6H$) has a very important effect on J_{c0}, compared to that of the oxygen deficiency ($6H$), while H_0 is strongly and equally influenced by both treatments. These simple observations help us to relate J_{c0} and H_0 to the microstructure and to the superconducting properties of the grains.

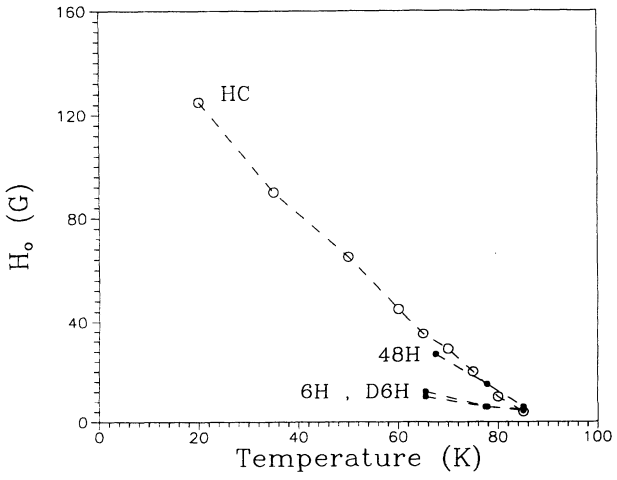

FIG. 4. H_0 as a function of temperature for $D6H$, $6H$, $48H$, and HC. The dashed lines are guides to the eye.

J_{c0} is the local critical current density in zero field. More precisely, it is the average current density needed to depin a single intergrain vortex. Following the analysis of Lobb *et al.*,[8,9] this depinning current density is related to the current density of a single junction, J_0(T), given by the Ambegaokar-Baratoff equation.[26] $J_{c0}(T)$ can then be expressed as this $J_0(T)$ multiplied by a factor (f) taking into account the strength and type of intergrain pinning centers:[7,9]

$$J_{c0}(T) = f\frac{\pi\Delta(T)}{2eR_N}\tanh\left(\frac{\Delta(T)}{2k_BT}\right), \tag{3}$$

where $\Delta(T)$ is the superconducting gap of the grains and R_N is the normal resistance of the junctions. Since there must be some distributions of dimensions, normal resistances and microstructure defects[9] in our materials, an adequate average of all the contributions is needed. Moreover, Eq. (3) is valid only when the grains are identical on each side of the junction. Because the $YBa_2Cu_3O_7$ grains are anisotropic and they are ramdomly oriented, one has to include an anisotropy factor and take the average over the relative orientation distribution. We add here that $J_0(T)$ can also be influenced if the Josephson junction is made of two superconductors in the strong-coupling limit ($2\Delta_0/k_BT_c > 3.52$) thus influencing $J_{c0}(T)$. Both features, the anisotropy (different gaps) and the strong-coupling case, are treated in chap. 3 of Ref. 25. All this leads to the conclusion that the temperature dependence of J_{c0} is a complicated average of the contributions listed above.

An interesting feature of our data is the effect of air degradation ($D6H$) compared to the oxygen deficiency ($6H$) on J_{c0}(T). We ascribe the significant decrease of J_{c0} for $D6H$ to the appearance of the green phase (Y_2BaCuO_5) during the degradation process, as seen using an optical microscope. Even after the 48-h treatment in UP O_2 , an incomplete recovery of the saturated properties ($48H$) is observed, which is indicative of an irreversible degradation. This increases the normal resistance of the junction (R_N) and a decrease of J_{c0} follows.

We must now deal with H_0 and its initial positive curvature near T_c. This parameter is often taken to be a constant for a fixed temperature and to be sample dependent.[27] Only few authors[28,29] have attempted to explain its physical meaning. In a previous paper,[22] we stated that H_0 is a measure of the field at which $J_{cj}(H)$ begins to decrease. When $H \ll H_0$, the flux lines are well separated and no vortex-vortex interaction is expected, since the intervortex distance, say a_0 , is larger than λ_J, the intergrain penetration depth.[30] In this condition, all the vortices find a pinning site. As the local field increases, the density of flux lines increases and reaches a state such that all the pinning centers are occupied (perfect matching): this defines a field H_0^*. The next flux line that is added cannot be pinned directly and must find an equilibrium position in the flux line network. This flux line is then easier to depin and one expects the corre-

sponding threshold magnetic field (H_0^*) to correspond to the first decrease of J_{cj} with H and to be related to H_0 with the same temperature dependence. If we evaluate this magnetic field in the case where $\lambda_J > r_g$ (r_g: mean grain radius) as shown in Fig. 5, we first note that N_g grains are embedded in a single flux quantum: the value of N_g is then given approximately by the ratio λ_J^2/r_g^2. Since the flux is concentrated in the intergrain region and at the surface by the grains within the mean London penetration depth λ_g (the interior of the grains being completely screened), each grain contributes an area $A_g \sim 8r_g\lambda_g$ to the total area embraced by the flux quantum. This allows an evaluation of H_0^* (see also Ref. 14):

$$H_0^* \equiv \frac{\phi_0}{N_g A_g} \sim \frac{\phi_0 r_g}{8\lambda_J^2 \lambda_g}, \tag{4}$$

where ϕ_0 is the quantum of flux. In Eq. (4), λ_J and λ_g are both proportional to $(1-T/T_c)^{-1/2}$ near T_c, such that $H_0^* \propto (1-T/T_c)^{3/2}$, in qualitative agreement with the observed positive curvature. Since λ_J varies as $J_0(T)^{-1/2}$ (see Refs. 7 and 31), we expect H_0^* (and H_0) to be influenced by an increase of the normal resistance of the junctions (H_0^* should then be proportional to R_N) as seen with $D6H$: a further indication that the normal resistance of the junctions increases with this degradation is the higher 100-K resistivity for $D6H$ (see Table I). It is also possible to affect H_0 by changing the oxygen content at the grain surface (as in $6H$), thus increasing λ_g. We must note here that J_{c0} for $6H$ is not significantly different from the $48H$ one. It indicates that most of the oxygen desorption during the 900 °C step occurs at the grain surfaces exposed to the ambient atmosphere (voids) and that the oxygen level remains high at the grain boundaries.

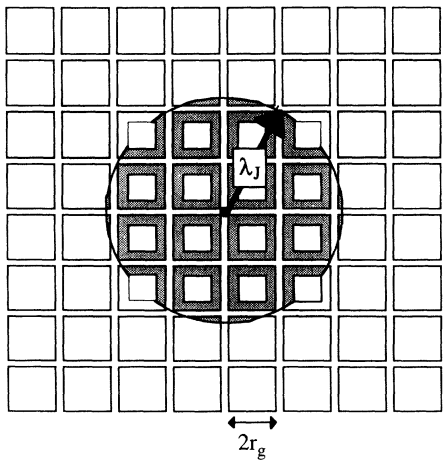

FIG. 5. Schematic of superconducting grains embedded in a flux quantum in the case $\lambda_J > r_g$.

The effect of H_{c1j}

In the calculations of Ref. 15, the intergrain lower critical field H_{c1j}, was neglected. As shown by LeBlanc,[16] it can contribute significantly to I_c if H_{c1j} is comparable to the characteristic fields obtained from the critical-state model (for example, H_p): this happens when the thickness of the slab is very small as in our case. Looking at the contribution at zero applied field, we obtain:

$$I_{c0} = 2Y(H_p + H_{c1j}). \tag{5}$$

To evaluate H_{c1j} at 67.5 K for $48H$, we interpolate the HC parameters to obtain J_{c0} and H_0. We then use these parameters to calculate the $I_c(H_a)$ curve. The result is shown in Fig. 2(b). We observe that this theoretical curve is well below the experimental one, which is indicative of the effect of H_{c1j}. The difference between the two values of I_{c0} gives a direct evaluation of H_{c1j}. We find $H_{c1j} \approx 1.3$ G. This contribution decreases as one approaches T_c and it becomes difficult to observe its effect.

Finally, we want to comment on the presence of H_{c1j}. When one adds intergrain silver (Ag) to these materials,[32] one observes a marked decrease in the width of the low-field hysteresis loop (ΔM), while the critical current (density) at zero applied field seems to remain constant or even to increase. Recalling that in the simple Bean model,[33] ΔM is proportional to J_c (here, it is J_{cj}), one concludes that the intergrain critical current density is depressed by the dilution of the volume fraction of grains with Ag. This will mainly influence H_0. However, the presence of Ag improves the junction contacts, which can result in an increase of H_{c1j} through an enhancement of J_{c0} and a reduction of λ_J.

SUMMARY

In this paper, we demonstrate the applicability of the general critical state model GCSM to the description of the magnetic and transport properties of polycrystalline $YBa_2Cu_3O_7$ in low fields (the intergrain regime). We find an agreement between the fitting parameters from the critical current of a thin slab and the ones from the field penetration in a hollow cylinder, both as a function of applied magnetic field. The three corresponding parameters, n, H_0, and J_{c0}, can be ascribed to the details of the microstructure (as the mean grain radius, the relative grain orientation, the mean orientation of the junction interfaces relative to the local field) and the general electronic and superconducting properties (as the junction normal resistance, the mean London penetration depth, the gap anisotropy, and the strong coupling).

We find that the various heat treatments can influence these parameters. The oxygen deficiency (at the surface of the grains) affects the mean London penetration depth and thus H_0. The air degradation increases

mainly the normal resistance of the junctions, and therefore decreases both J_{c0} and H_0. No effect on n is found suggesting that it is independent of the superconducting properties of the grains.

Finally, we find that the presence of H_{c1j} becomes increasingly important when dealing with very thin slabs of increasing superconducting quality (e.g., decreasing temperatures).

ACKNOWLEDGMENTS

We are indebted to C. Julien for her technical support throughout this project. The authors would like to thank NSERC (Canada), FCAR (Québec) and the Centre de Recherche en Physique du Solide for their financial support.

* Present address: E.L. Ginzton Laboratory, Stanford University, Stanford, CA 94305-4085.

[1] J.E. Evetts and B.A. Glowacki, Cryogenics **28**, 641 (1988).
[2] S. Senoussi, M. Oussena, and S. Hadjoudj, J. Appl. Phys. **63**, 4176 (1988).
[3] K.-H. Müller, Physica C **158**, 69 (1989).
[4] F. Stucki, J. Rhyner, and G. Blatter, Physica C **181**, 385 (1991).
[5] J.W. Ekin, H.R. Hart, Jr., and A.R. Gaddipalti, J. Appl. Phys. **68**, 2285 (1990).
[6] H. Dersch and G. Blatter, Phys. Rev. B **38**, 11 391 (1988).
[7] J.R. Clem, Physica C **153-155**, 50 (1989).
[8] C.J. Lobb, D.W. Abraham, and M. Tinkham, Phys. Rev. B **27**, 150 (1983);
[9] M.B. Cohn, M.S. Rzchowski, S.P. Benz, and C.J. Lobb, Phys. Rev. B **43**, 12 823 (1991).
[10] R. Vaccarone, J. Supercond. **6**, 161 (1993).
[11] S. Senoussi, J. Phys. III (France) **2**, 1941 (1992).
[12] P. Fournier, M. Oussena, and M. Aubin, Cryogenics **33**, 333 (1993).
[13] P. Fournier and M. Aubin, Physica B **189-191**, 1388 (1994).
[14] P. Fournier and M. Aubin, Phys. Rev. B **49**, 15 976 (1994).
[15] K.-H. Müller, D.N. Matthews, and R. Driver, Physica C **191**, 339 (1992).
[16] M.A.R. LeBlanc, Cryogenics **32**, 813 (1992).
[17] D. St-James, G. Sarma, and E.J. Thomas, *Type II Superconductivity* (Pergamon, Oxford, 1969).
[18] See, for example, C.A. D'Ovidio, J.E. Fiscina, and D.A. Esparza, J. Appl. Phys. **69**, 8265 (1991); D.N. Matthews and K.-H. Müller, *ibid.* **72**, 2964 (1992).
[19] M. Xu, D. Shi, and R.F. Fox, Phys. Rev. B **42**, 10 773 (1990).
[20] A.M.T. Bell, Supercond. Sci. Technol. **3**, 55 (1990).
[21] Y. Sun and H. Yang, Cryogenics **31**, 760 (1991).
[22] P. Fournier and M.Aubin, Rev. Sci. Instrum. **65**, 788 (1994).
[23] J.W. Ekin, Appl. Phys. Lett. **55**, 905 (1989).
[24] R.-L. Peterson and J.W. Ekin, Physica C **157**, 325 (1989).
[25] A. Barone and G. Paterno, *Physics and Applications of the Josephson Effect* (Wiley, New York, 1982).
[26] V. Ambegaokar and A. Baratoff, Phys. Rev. Lett. **10**, 486 (1963).
[27] Y.B. Kim, C.F. Hempstead, and A.R. Strnad, Phys. Rev. Lett. **9**, 306 (1962).
[28] P.W. Anderson, Phys. Rev. Lett. **9**, 309 (1962).
[29] J.A. Hulbert, Brit. J. Appl. Phys. **16**, 684 (1965).
[30] T.L. Hylton and M.R. Beasley, Phys. Rev. B **39**, 9042 (1989).
[31] M. Tinkham, *Introduction to Superconductivity* (McGraw-Hill, New York, 1975).
[32] J. Jung, M.A.-K. Mohammed, S.C. Cheng, and J.P. Franck, Phys. Rev. B **42**, 6181 (1991).
[33] C.P. Bean, Rev. Mod. Phys. **36**, 31 (1964).

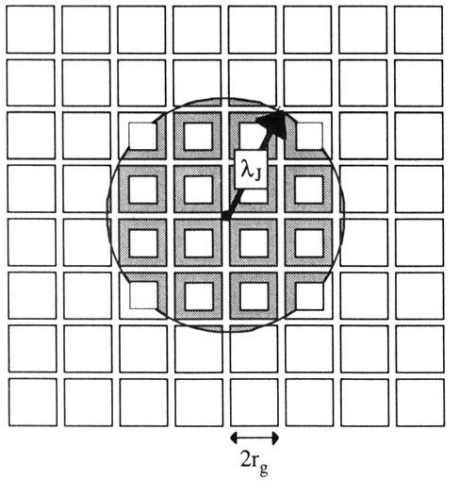

FIG. 5. Schematic of superconducting grains embedded in a flux quantum in the case $\lambda_J > r_g$.